Hybrid Cross-Linked Bio Polymer-Epichlorohydrin/Fe_3O_4 Nanocomposite for As(V) Adsorption: Kinetic, Isotherm, Thermodynamic, and Mechanism Study

Nagarajan, Vijayanand*[+]***; Ganesan, Raja***

Department of Chemistry, Paavai Engineering College (Autonomous), Namakkal, TN, INDIA

Govindaraj, Prabha

Department of Applied Science and Technology, Alagappa College of Technology, Anna University, Chennai, INDIA

ABSTRACT: *In the present work, iron-doped particle Carboxymethylchitosan nanocomposite cross-linked with epichlorohydrin (CMC-EPC/INC) were prepared, by a chemical precipitation method, characterized and evaluated for the removal of As(v) from an aqueous solution. The adsorbent was characterized by FT-IR, XRD, and SEM. Key parameters, including adsorbent dosage, pH, temperature, initial ion concentration, and contact time were investigated and found to be 0.4g, pH 4, 308K, 10 mg/L, and 120 min, respectively. Mechanism study reveals the availability of amino groups in biopolymer, which act as active adsorption sites towards the arsenic anion. On evaluating isotherm models of Langmuir, Freundlich, Temkin, Elovich, Redlich-Peterson, and Dubbin-Radushkovich, it was found that the Langmuir isotherm model fitted better compared to other models having a maximum adsorption capacity of 28.99mg/g, a high regression coefficient value of 0.9988, least chi-square value of 0.1781 and validated by D-R isotherm also. The process was found to follow monolayer adsorption and pseudo-second-order kinetics. Thermodynamic parameters such as ΔS, ΔH, and ΔG indicated the spontaneous, endothermic, and physisorption nature of adsorption. Competing anions did not cause a significant reduction in the adsorption behavior of arsenic. Successful regeneration of the adsorbent implies its applicability to the removal of arsenic from real-life wastewater.*

KEYWORDS: *Arsenic; Hybrid Biopolymer nanocomposite; Epichlorohydrin; D-R Isotherm; Thermodynamic.*

INTRODUCTION

Arsenic is a pervasive element in the environment and has been known as a notorious toxic substance to man and living organisms for centuries [1]. Groundwater Arsenic is primarily associated with oxidative weathering and geochemical reactions. The major role in the mobilization of arsenic is played by the amount of reactive carbon in the

***** *To whom correspondence should be addressed.*
+ *E-mail: vijayanandnagarajanpec@paavai.edu.in*
1021-9986/2022/10/3419-3432 14/$/6.04

sediments [2]. Arsenic contaminated groundwater affects over 100 million people in Bangladesh, West Bengal, China, Mexico, Chile, Myanmar, and United States [3]. Long-term exposure to arsenic in drinking water causes skin diseases (pigmentation, dermal hyperkeratosis, skin cancer), cardiovascular, neurological, renal, respiratory and black foot diseases, as well as lung, liver, kidney, and prostate cancers [4].To protect public health, the World Health Organization has seta provisional guideline limits of 10µg/L for arsenic [5] in drinking water which was afterward adopted by the European Union and India. The removal of Arsenic by various methods has been adequately reviewed [6]. Co-precipitation, flotation, ion exchange, ultra-filtration, and reverse osmosis have received more attention due to its high concentration efficiency. Several adsorbents have been found suitable for arsenic removal including activated carbon [7], activated alumina [8], red mud [9], etc., In the last decade developments in the knowledge of biosorption exposed high adsorption capacities, low costs and renewability of natural biosorption materials [10]. However, challenges are countered for biosorbents with high adsorption capacity, low cost, and as well as in understanding the mechanism of biosorption with heavy metals [11]. Chitosan is produced from N-deacetylation of chitin, a major component of crustacean shell and fungal biomass, readily available from seafood processing wastes. Due to the presence of hydroxyl and an amine group, chitosan has been found to possess good sorption capacity for many heavy metal ions from wastewater [12] through complexation reactions. Due to the deceasing property of chitosan in practical application, it requires chemical modification in order to recover the hydrophilic property and further enrich the adsorption capacity for metal ion adsorption [13]. Carboxymethyl chitosan (CMC) can be an effective substitute for chitosan owing to its amphiprotic nature, which contains hydroxyl (-OH), carboxyl (-COOH) and amine ($-NH_2$) groups in the molecule. But, due to its poor chemical stability and other limitations [14], crosslinking reaction is carried out with agents like, glutaraldehyde, glyoxal, and ethylene glycol diglycidyl ether[15] (EDGE). Still, the restriction of these cross-linker agents arises from the blocking of amino (NH_2) functional group in CMC backbone. Therefore, epichlorohydrin (EPC) as a mono-functional cross linking agent was an effective substitute that will not bind to amino groups in CMC biopolymer [16]. Where, these functional groups can improve the hydrophilic property of CMC and provide enough adsorption sites for increasing adsorption capacity. Nowadays, the CMC-EPC and /or their composite biomaterials were synthesized and applied for the removal of synthetic dyes and heavy metals in waste water [17]. However, the fact of high desirability exist between inorganic arsenic species and iron tends to advance the utility of Fe (III)-bearing materials like goethite and hematite [18], ferrihydrite [19], and iron-doped activated carbons [20] for arsenic adsorption. Studies also recognized the applicability of CMC-Fe nanoparticles for the removal of hexavalent chromium. Thus, the objective of the present study is to prepare a hybrid composite biopolymer of crosslinked epichlorohydrin/Fe_3O_4 nanocomposite (CMC-EPC/INC) as a promising biosorbent for the removal of As(V). The adsorption key parameters such as adsorbent dosage, initial metal ion concentration, solution pH, working temperature were investigated. The Langmuir, Freundlich, Temkin, Elovich, Redlich-Peterson (R-P), and Dubinin-Radushkovich (D-R) isotherm models were applied to evaluate the adsorption equilibrium. Kinetic study was also performed using pseudo-first, second-order, and intraparticle diffusion models. The thermodynamic properties were carried out to find spontaneous nature by Van't Hoff equation. Finally, the adsorption mechanism was adequately discussed.

EXPERIMENTAL SECTION

Chemicals & Reagents

Carboxymethylchitosan (CMC, MW= 2.65×10^5), with an 80% deacetylation degree, Epichlorohydrin (EPC), Ferric chloride hexahydrate ($FeCl_3.6H_2O$), Ferrous chloride tetrahydrate ($FeCl_2.4H_2O$), Sodium hydrogen arsenate ($Na_2HAsO_4.7H_2O$),1-ethyl-3-carbodiimide hydrochloride (EDC), N-hydroxyl succinimide (NHS), Sodium hydroxide and acetic acid were of analytical grade, acquired from Sigma Aldrich. Stock As(V) solution (1000mg/L) were prepared from sodium hydrogen arsenate. All the reagents and glassware were prepared with de-ionized water.

Preparation of Fe_3O_4 nanoparticles.

Synthesis of Fe_3O_4 nanoparticles was carried out according to the procedure described away [21]. To prepare Fe_3O_4 nanoparticles 0.02 moles of $FeCl_3.6H_2O$ and 0.01 moles

0.01 moles of $FeCl_2.4H_2O$ were dissolved in 100mL of deoxygenated deionized water. Chemical precipitation was achieved at 30ºC under vigorous stirring by the addition of 1M NaOH after 60min. Then it was heated to 60ºC for 3h under the pH±12. After cooled the solution to room temperature, the precipitate was collected by a magnet and washed with deionized water until the pH reached neutral. Finally, it was washed with acetone and dried in an oven at 60ºC for 24h.

Synthesis of CMC-EPC/Fe_3O_4 Nanocomposite

1g of CMC was dissolved in acetic acid (50 mL, 5% v/v), and the mixture was sonicated at room temperature for 3h. Then 0.6g of magnetic nanosized ferroferric oxide was added to the colloidal solution and the mixture was left for 24h at room temperature with vigorous stirring to ensure dissolution of CMC and incorporation of Fe_3O_4 nanoparticles in the CMC matrix. The resultant solution was injected into a 100mL sodium hydroxide (0.5 M) by syringe needle (10 mL) as drops, where the CMC-Fe_3O_4 (MCMC) beads formed instantaneously. The fresh beads were washed with distilled water plenty for the removal of excess sodium hydroxide solution. The crosslinking steps were carried out by dissolving 1 g of MCMC beads in 60 mL of ultrapure water followed by adding 0.6 g of EDC and 0.8 g of NHS at pH 5-6 in order to activate the carboxyl groups of MCMC. After 1 h, 1% epichlorohydrin (100mL) was added to the beads with gentle stirring in water bath at 40ºC for 24 h. Then the crosslinked (CMC-EPC/INC) beads were washed many times with distilled water, air dried and ground using a mortar and dried constantly in the oven. Finally, the prepared adsorbent was sieved to get a uniform particle size of less than 250µm for study.

Batch adsorption experiments.

Batch experiments were carried out in 100mL polyethylene bottles with 50mL of As solution having an initial concentration of 10mg/L. The investigation carries the effect of various parameters such as temperature (20-50ºC), pH (2-10), reaction time (5min-5h), and adsorbent dosage (0.1-2g/50mL) in order to find the maximum uptake of arsenic ions. Samples were collected at fixed intervals and the adsorbent was removed by centrifugation at 6000 rpm for 6 min. The supernatant was analyzed for As(v) removal by AAS. Blanks were used for control in all the experiments. The amount of arsenic adsorbed (mg/g) was determined by the following equation.

$$q_e = (C_o - C_e) \times {}^{V}/_{m} \quad (1)$$

Where C_0 and C_e are the initial and equilibrium concentrations of the metal ion (mg/L), m is the dry mass of iron-doped chitosan (g) ,and v is the volume of the solution (L). The % removal of As(v) from aqueous solution was calculated by the following equation;

$$\text{Removal (\%)} = [(C_0 - C_e)/C_0] \times 100 \quad (2)$$

The maximum adsorption was found at the equilibrium condition of pH 4, adsorbent dosage 0.4 g/50mL, temperature 35ºC, and reaction time of 120 min. Adsorption isotherm studies were conducted by varying the initial As(v) concentrations (2-250 mg/L) at different temperatures (25, 30 and 35ºC).

Analytical Measurements

Fourier Transform InfraRed (FT-IR) spectrometer to identify the functional groups of CMC-EPI/INC before and after adsorbed As(v) with KBr discs in the range of 400-4000cm^{-1} on Jasco-4200**.** The porosity and Morphology of the composite were examined by N_2 adsorption/desorption isotherm at temperature 77 (K) using Micromeritics ASAP 202 analyzer and JOEL JSM-6360 scanning electron microscope at 25kV respectively. For crystalline phase identification, X-Ray powder Diffraction (XRD) patterns were recorded on a D8 FOCUS X-ray diffraction spectrometer (Bruker, Germany) with Cu Kα radiation from 10º to 80º. A pH-potentiometric titration method, reported by *Vieira* and *Beppu* [22], was carried out to determine the amino group content in the biosorbent. Shimadzu AA 7000 model Atomic Absorption Spectrometer (AAS) was used to measure the concentration of adsorbed arsenic at 193.7nm with an air-acetylene flame type.

RESULTS AND DISCUSSION

Mechanism and characterization of the Fe_3O_4/CMC nanocomposite

The preparation of the Fe_3O_4/CS nanocomposite by chemical precipitation method was reported elsewhere [23]. Dispersion of CMC and Fe_3O_4 was carried out in the first step of the mechanism resulting in the formation of Fe^{3+} and Fe^{2+}. The degree of deacetylation and the degree of dissociation of amine groups [24] decides the acid/base property of chitosan (pk_a). The second step outcomes in the preparation of $Fe(OH)_3$ and $Fe(OH)_2$ by the addition of NaOH. Therefore, the complex compound formed

Table 1: Surface area of cross-linked chitosan derivatives.

Chitosan derivative adsorbents	BET surface area (m^2/g)	References
La(III) loaded carboxylated cross-linked chitosan beads (LaCCB)	2.15	[25]
Fe(III) loaded carboxylated cross-linked chitosan beads (FeCCB)	2.09	[26]
Zr(IV) loaded carboxylated cross-linked chitosan beads (Zr CCB	2.32	[27]
Protonated cross-linked chitosan beads (PCB)	2.05	[28]
Glutaraldehyde cross-linked chitosan beads (chitosan-GLA)	1.45	[29]
Fe(III) loaded epichlorohydrin cross-linked carboxymethylchitosan (CMC-EPC/INC)	2.85	This Study

in which Fe^{2+}ions act as the metal center, while $–NH_2$ and –OH are the ligands of the CMC. The reaction of Fe_3O_4 formation is as follows:

$$Fe^{2+} + 2Fe^{3+} + 8OH^- \rightarrow Fe_3O_4 + 4H_2O \quad (3)$$

Porosity and SEM analysis

The BET surface area analysis shows that the adsorbent has a surface area of 2.85 (m^2/g). The nitrogen sorption measurements were performed to investigate the textural characteristics of the resultant CMC-EPC/INC@As(V) nanocomposite. Table 1 represents the surface areas of various modified chitosan beads with various crosslinkers. It is evident that the chitosan nanocomposite prepared through the Fe_3O_4 dissolution epichlorohydrin method has a significantly high surface area compared to other adsorbents.

The nitrogen isotherms in Fig.1 resulted in a type IV shape with an H_2 hysteresis loop in the range of 0.38–0.98 relative pressure. These results suggest that the CMC-EPC/Fe_3O_4@As(V) nanocomposite are characterized by large mesoporous structures with pore sizes of 20–30 nm, where the pore volume are characterized by "small" mesopores (<4 nm in diameter), "medium" mesopores (4–10 nm) and "large" mesopores (>10 nm). These variations in hysteresis and pore size distribution may be ascribed to the role played by chitosan in designing the pore structure of the nanocomposite, which is based on incorporating Fe_3O_4 and epichlorohydrin structures into a single material. The surface morphology of the composite examined by the scanning electron microscope indicates, in Fig. 2 (a), that the adsorbent is porous in nature. Fig.2 (b) illustrates the SEM images after As(V) loadidisplayinglays more white patches entitle the adsorbent complexes with arsenic ions.

Potentiometric analysis

The actual content of amino ($-NH_2$) group was analysed by the potentiometric titration in the molecular structure of

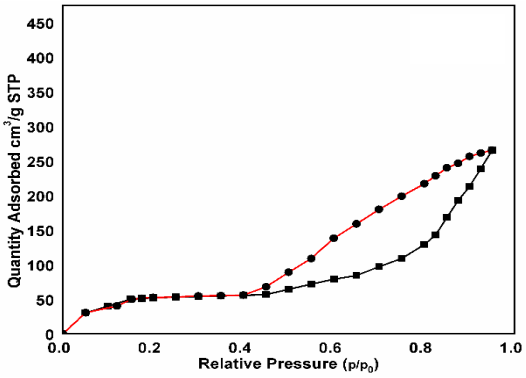

Fig. 1: Nitrogen adsorption–desorption isotherms of CMC-EPI/INC @As(V)nanocomposite.

CMC-EPI/INC is 40.1%. In-general, the interaction between Lewis acidic and basic sites of ferrous ferric oxide and amino group in CMC respectively, decreases amino ($-NH_2$) group content in the matrix of CMC [30].

The cross-linking of EPI, which basically reacts with the primary alcoholic group ($-CH_2OH$) at position C-5 of CMC's pyranose ring [31], does not responsible for the decrease in the amino ($-NH_2$) group content of CMC. Therefore, it is evidenced by the potentiometric titration test that the adsorbent maintains a comparatively high amino ($-NH_2$) group content, which a major role in the adsorption of arsenic anion by the influence of electrostatic attraction between positively charged CMC-PI/INC and negatively charged arsenic anion.

XRD analysis

XRD pattern of Fe_3O_4, MCMC and CMC-EPI/INC were shown in Fig.3. The orientation and relative intensities of diffraction peaks matched well for prepared Fe_3O_4,Fig. 3(a), with Jade PDF card (65-3107) Fig.3(b). However, blurred diffraction peaks were observed in MCMC, Fig.3(c) and CMC-EPI, Fig. 3(d), was probably

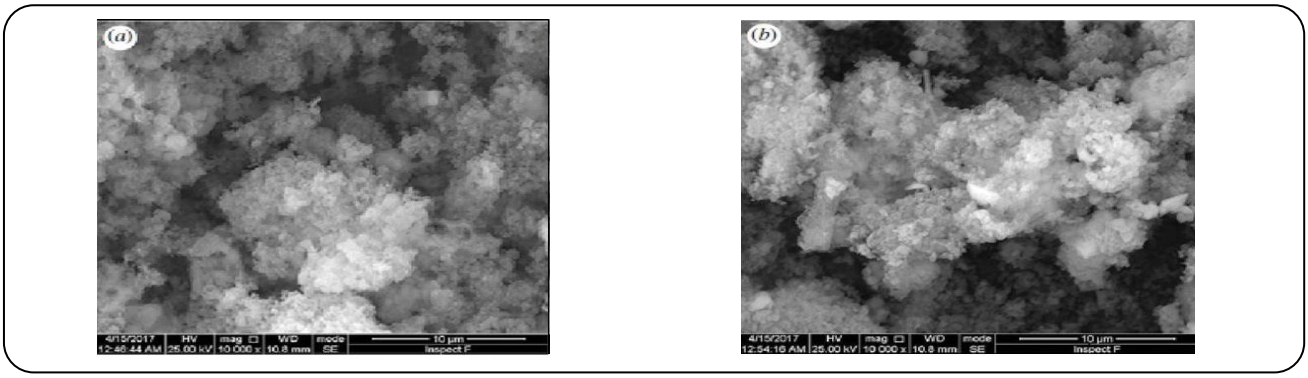

Fig.2: SEM Images of CMC-EPI/INC composite a) before and b) after As(V) adsorption.

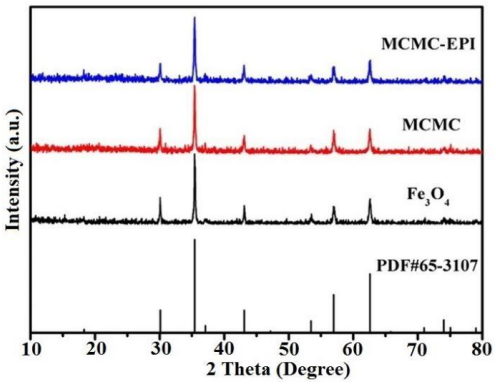

Fig. 3: XRD Image of (a) Fe_3O_4 (b)MCMC.

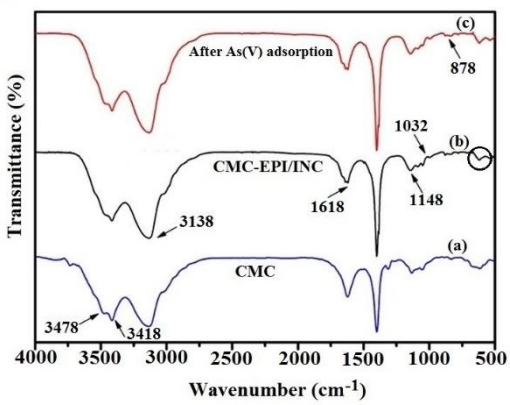

Fig. 4: FT-IR spectrum of (a) CMC (b) CMC -EPI/INC before and (C) after As(V) adsorption.

due to amorphous nature of CMC and EPI in MCMC and MCMC-EPI respectively, but evident the presence of Fe_3O_4 by indistinct peaks observed at 2θ =30º,36º, 44º, 53º, 57º,63º,71º and 74º.These peaks reflect that the composite has emphasized the integration of Fe_3O_4 into CMC.

FT-IR analysis

The existence of important functional is confirmed by the examination of the FT-IR spectra of the pure CMC, CMC-EPI/INC before and after As(V) adsorption were displayed in Fig. 4. The IR spectrum of CMC in Fig.4 (a), shows a distinct peak at 3478 cm^{-1},3418 cm^{-1},3138 cm^{-1} and 1618 cm^{-1} were attributed to the symmetrical, asymmetric stretching vibration of and $–NH_2$ group and stretching vibration of O-H , with the effect of hydrogen bonds, and C = O in amide respectively. The peaks at ~1148 cm^{-1} and ~1032 cm^{-1} in Fig.4 (b), correspond to the stretching of C-O-C and C-O bonds respectively, resulting in the formation of covalent bonds due to the reaction between EPI with the carbon atoms of the hydroxyl groups in CMC, which causes the opening of the epoxide ring of EPI and the releasing of a chlorine atom [32]. The bands around 600-700 cm^{-1} is assigned to the bending vibration of Fe-O-Fe bond. The appearance of a new band ~878 cm^{-1} shown in Fig.4 (c), corresponds to the existence of arsenic anion.

Determination of optimum adsorption capacity for CMC-EPI/INC

The optimum adsorption capacity of the prepared adsorbent was determined by varying the parameter conditions from the batch experiments as described above. The effect of each parameter on the adsorption process is discussed below in detail.

Effect of pH

In the present study, the effect of solution pH on the adsorption of As(V) was investigated at different pH from 2 to 12 at a temperature of 298K having an initial metal ion

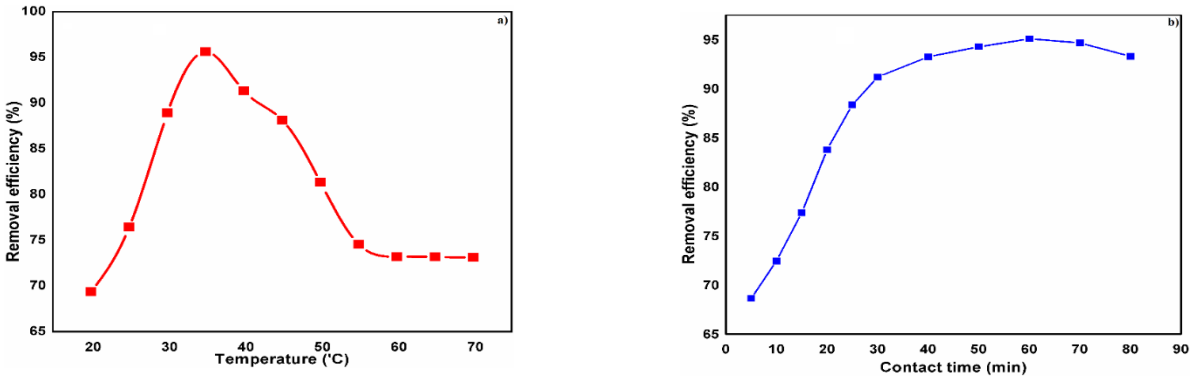

Fig. 5: Effect of (a) temperature and (b) contact time on the adsorption of As(V) having an initial concentration of 10mg/L at pH=6.5.

concentration of 10ppm. The results show that initially the amount of As(V) adsorbed onto CMC-EPI/INC composites increases with an increase in the pH both attaining maxima at pH 6.5. With further increase in pH, the net adsorption of metal ions onto adsorbent does not increase because of the formation of metal hydroxide in alkaline medium [33]. At lower pH, adsorption is not prominent due to a higher concentration of H+ ions which competes with As(V) ion adsorption onto CMC-EPI/INC.

Effect of temperature

In order to study the effect of temperature on the adsorption process experiments were carried out at various temperatures from 25ºC to 55ºC, at an interval of 5ºC,in the same procedure as described above.From the plot, Fig. 5, it was observed that initially, the adsorption increased on increasing with temperature with maximum adsorption at 35ºC and there on decreased with further increase in temperature. This can be attributed to the fact that initially when temperature increases the thermal energy of the metal ions also increases which in turnincreasese the possibility of contact between the vacant sites of the adsorbent and the metal ions. However, on increasing the temperature further the thermal vibration of the metal ions become much faster than the adsorbent-metal ion interaction resulting in the release of metal ions back into the solution.

Effect of contact time

Contact time between the adsorbate molecule and the adsorbent surface has an intense effect on the adsorption capacity. Initially, when all the adsorbent sites are vacant, the adsorbate molecule attaches to the vacant sites as soon as the metal ions come in contact with them thereby showing a gradual increase in the adsorption with time till a maximum is attained at 60 min as shown in Fig.6. Thereafter no further increase in adsorption is observed, due to fact that when all the adsorbent sites are occupied a dynamic equilibrium is attained in which the number of molecules being adsorbed equals the number of adsorbate molecules being desorbed [34].

Effect of initial concentration

The initial concentration of the adsorbate molecule affects the rate of adsorption to a great extent. At low initial concentrations, a lesser number of collisions occur between the adsorbate molecules and the adsorbent which increase with the increase in the adsorption capacity up to an initial concentration of 10mg/L for As(V) ion. There is no further increase in adsorption with increasing initial ion concentration due to the attainment of the dynamic equilibrium between free adsorbate ions in solution and adsorbed metal ions.

Equilibrium isotherm

The adsorption of As(V) onto CMC-EPI/INC at different temperatures is shown in Fig.S1. It exposes the adsorption is endothermic and takes place by diffusion and complexation processes respectively, due to the increasing diffusion rate of As(V) onto the sorbent surface and the growing rate of complexation in the adsorbent [35].

Adsorption mechanism

Generally arsenate, As(V), exists as $H_2AsO_4^-$, $HAsO_4^{2-}$, and AsO^{3-} in surface water at natural and highly basic conditions respectively depending on pH. Predominantly

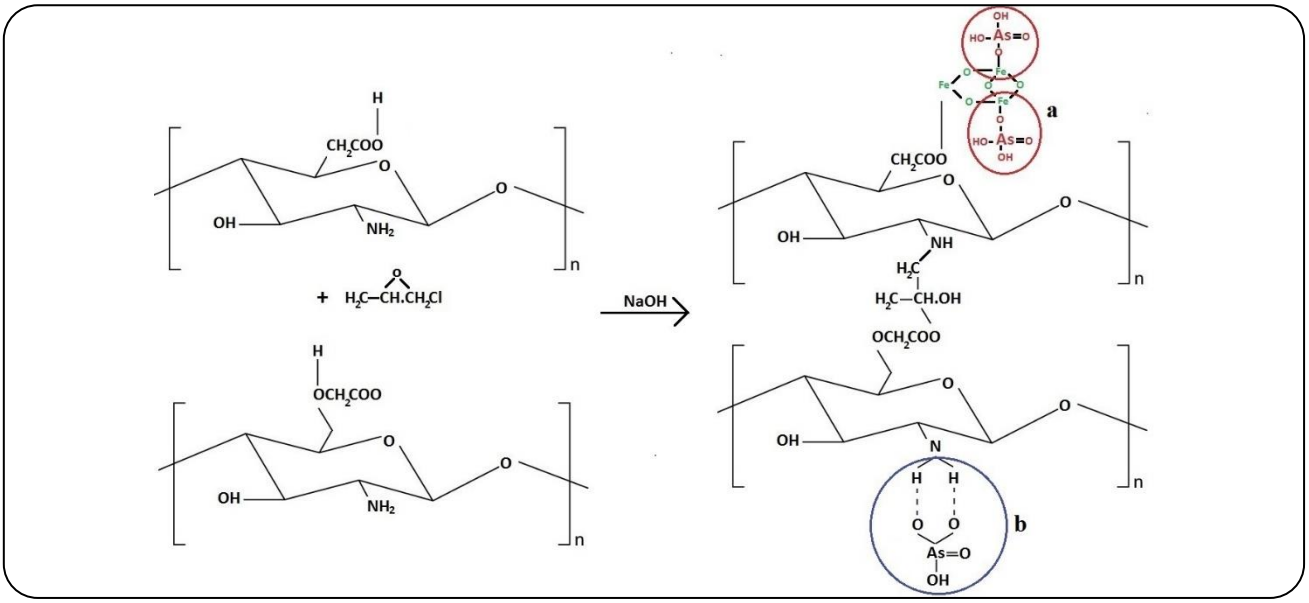

Fig. 6: Proposed Mechanism of As(V) adsorption onto CMC-EPI/INC composite.

As(V) will prevail in two form as $H_2AsO_4^-$ and $HAsO_4^{2-}$ in surface water under aerobic oxidation, by the reaction between H_3AsO_4 and H_2O.

$$H_3AsO_4 + H_2O \leftrightarrow H_2AsO^{-4} + H_3O^+ \ (K_1 = 10^{-2.19}) \quad (4)$$

$$H_2AsO^{-4} + H_2O \leftrightarrow HAsO_2^{-4} + H_3O^+ \ (K_2 = 10^{-6.94}) \quad (5)$$

Therefore, $H_2AsO_4^-$ and $HAsO_4^{2-}$ anions adsorption is focused onto the biosorbent for As(V) removal. There are two adsorption sites, amino group (-NH_2) and $Fe^{2+}$of Fe_3O_4, are available on the surface of the CMC-EPI/INC composite that can be involved in different types of interactions, as shown in Fig.6. One of the mechanisms involves the electrostatic attraction, Fig.6 (a), considered as the most eventful attraction force take place between negatively charged arsenate ion of H_2AsO^{-4}, with positively charged Fe^{2+}, available on the CMC-EPI/INC surface. The adsorption mechanism also includes dipole-dipole H-bonding interaction in Fig.6(b), which occurred between hydrogen on the surface of CMC-EPI/INC and atoms of O in the arsenate anions of $HAsO_2^{-4}$.

Adsorption isotherms

The isotherm models, employed in the linear form [36] were shown in Table 2, and could be used to describe the sorption data, sorption mechanism, surface properties, and the affinity between sorbent and sorbate. The equilibrium parameters, linear regression analysis, and computed constants were shown in Table 3.

Langmuir isotherm

It represents the monolayer sorption on an energetically uniform surface. The maximum adsorption capacity, q_m=26.11-28.99mg/g, and higher regression coefficient, R^2=0.9988 were obtained from the relevant Langmuir isotherm plots (Fig. 7a), suggesting that the surface of the sorbent was homogenous. The dimensionless factor (R_L=1/1+ bC_o) was calculated as <1, indicatingfavorablee adsorption and following the monolayer adsorption process. The certainty of the isotherm were committed by the least RMSE and χ^2 values for the Langmuir model than other isotherm model values employed.

Freundlich isotherm

The isotherm describes the sorption on

an energetically heterogeneous surface and the exponential distribution of active sites and their energies [37]. The value of n (adsorption intensity) obtained, from the Freundlich model (Fig.7b) in the range 1-10 signifies the good performance of Fe_3O_4 doped CMC-EPI adsorbent towards As(V) adsorption.

Temkin Isotherm

The adsorption behavior between adsorbent and adsorbate is explained by this model by the assumption that the adsorption heat of all molecules decreases linearly

Table 2: The forms of different isotherms.

Model	Linear form
Langmuir	$\frac{C_e}{q_e}=\frac{1}{k_L q_m}+\frac{C_e}{q_m}$
Freundlich	$\log q_e=\log k_F+\frac{1}{n}\log C_e$
Temkin	$q_e=\beta \ln K_T+\beta \ln C_e$
Elovich	$\ln\frac{qe}{Ce}=\ln q_m-{q_e}/{q_m}$
R-P	$\ln\frac{C_e}{q_e}=\beta \ln C_e-\ln A$
D-R	$\ln q_e=\ln q_m-\beta\varepsilon^2$

with the increase in coverage of adsorbent surface characterized by uniform distribution of maximum binding energy (A,(L/g)). Fig. 7c and Table 3 show good agreement between experimental data and Temkin model equation between anionic and adsorbent surfaces.

Elovich isotherm

The model is based on a kinetic principle which assumes that the adsorption sites increase exponentially with adsorption, this infers multilayer adsorption. The isotherm parameters for this model were obtained from the plot (Fig.7d) relating $\ln q_e/c_e$ against q_e.The results, from Table 3, indicated that the elovich model is non-significant to this adsorption study.

Redlich-Peterson isotherm

The Redlich-Peterson (R-P) equation comprises three parameters and integrates the elements of the Langmuir and the Freundlich isotherms. In R-P equation, $k_{RP,}\,\alpha_{RP}$ and β are the R-P parameters, β lies between 0 and 1. If β=1, the equation reduces to Langmuir form. When k_{RP} and α_{RP} are greater than unity the equation can transform to the Freundlich form. The computed constants of R-P isotherm are obtained from the plot (Fig.7e). The Table 3 shows the values of β at different temperatures were nearer to unity than 0 and $k_{RP,}\,\alpha_{RP}$ values were lesser than unity, indicating that the isotherm was more impending the Langmuir than the Freundlich model. The context was also be confirmed by that the high regression coefficient of Langmuir (R^2=0.9988) than the Freundlich model (R^2=0.9898). Hence, the monolayer coverage process of adsorption by the composite was affirmed by the best fit of equilibrium data in both the R-P and the Langmuir isotherm models.

Table 3: Equilibrium parameters for As(v) adsorption.

Model	Parameters	Temperature (K)		
		298	303	308
Langmuir	$q_{m(mg/g)}$	26.11	27.38	28.99
	$k_{l(L/mg)}$	0.0594	0.0668	0.0941
	R^2	0.9644	0.9851	0.9988
	R_L	0.6274	0.5995	0.5152
	$RMSE$	0.3852	0.3526	0.2978
	χ^2	0.2943	0.2896	0.1781
Freundlich	$k_{f(mg/g)}$	1.4027	1.4276	1.5327
	η	1.9592	1.6489	1.8221
	R^2	0.9623	0.9821	0.9898
	$RMSE$	2.9651	3.1475	3.2541
	χ^2	5.9621	5.6254	4.9632
Temkin	β	4.4756	5.2804	5.2013
	$A/k_{T(L/mg)}$	1.1193	1.1518	1.2184
	$b(Jmol^{-1})$	0.5535	0.4771	0.4923
	R^2	0.9412	0.9483	0.9670
	$RMSE$	0.8766	0.9617	1.0313
	χ^2	2.8598	2.6928	3.2827
Elovich	$q_{E(mg/g)}$	9.4787	10.4493	12.1212
	$k_{E(L/mg)}$	1.0817	1.0825	1.1371
	R^2	0.9553	0.9537	0.9811
	$RMSE$	0.4856	0.5241	0.4738
	χ^2	1.6548	2.1749	2.0845
R-P	β	0.4615	0.4175	0.4523
	$\alpha_{RP\,(L/mg)}$	2.1302	2.4975	2.6706
	$k_{RP\,(L/g)}$	0.0816	0.0912	0.0921
	R^2	0.9810	0.9889	0.9958
	$RMSE$	1.5278	1.2564	1.0726
	χ^2	3.2189	2.8412	2.0945
D-R	$q_{m(mg/g)}$	11.9987	12.6822	12.8829
	β_{DR}	0.3718	0.2906	0.2547
	E_{DR}	1.1504	1.3117	1.4012
	R^2	0.8089	0.8122	0.8236
	$RMSE$	1.2347	1.5247	1.5561
	χ^2	2.1347	1.8524	1.2045

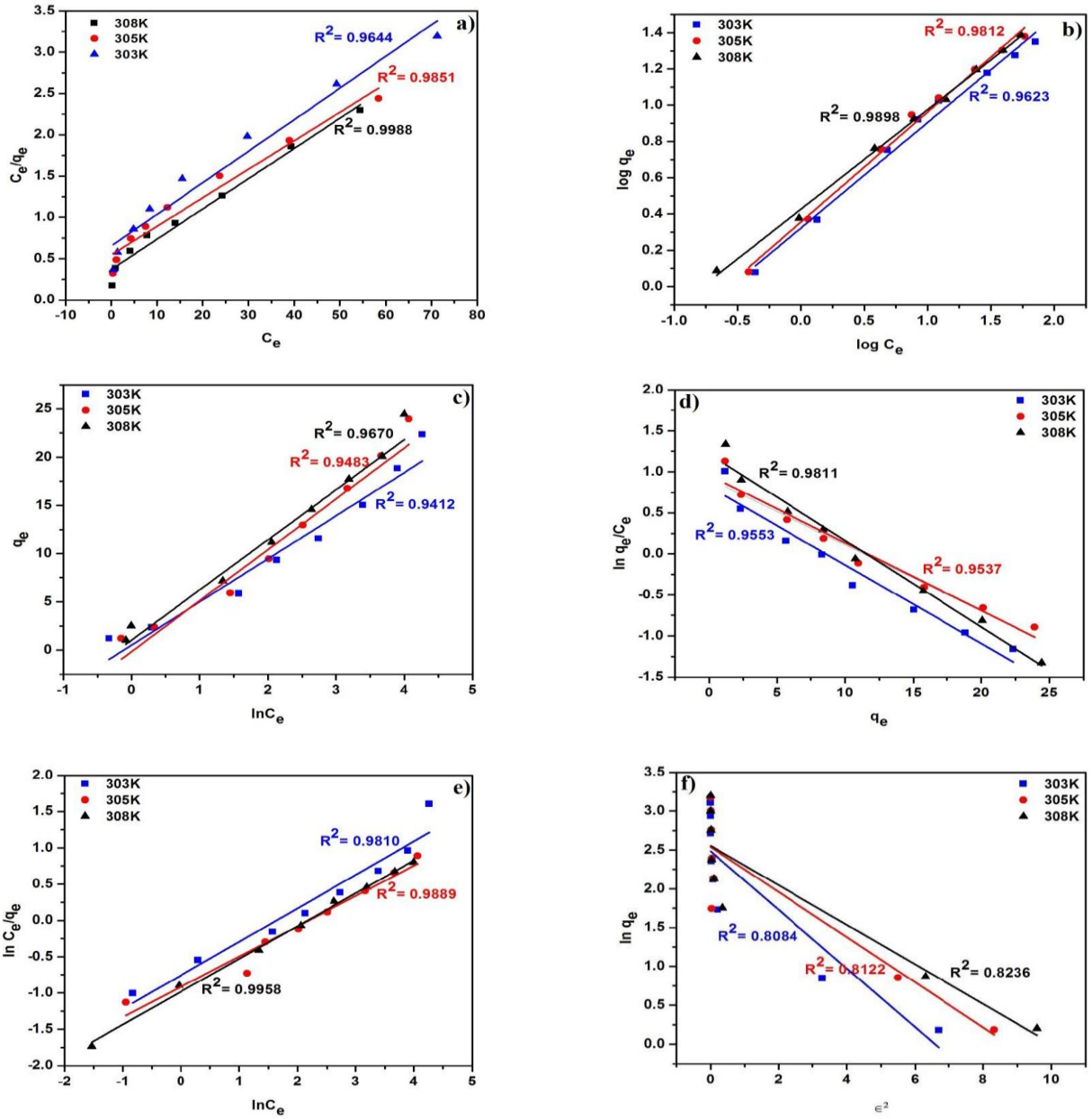

Fig. 7: Isotherm plots of (a) Langmuir (b) Freundlich (c) Temkin (d) Elovich (e) R-P and (f) D-R model for As(V) adsorption onto onto CMC-EPI/INC composite.

Dubinin-Radushkovich isotherm

The model in which adsorption follows a pore filling mechanism generally applied to differentiate between physical and chemical adsorption of metal ions by a semiempirical equation. The constant β gives the mean sorption energy, E_{DR} (kJ/mol) computed by the relation;

$$E_{DR} = \frac{1}{\sqrt{2\beta}} \qquad (6)$$

The values of β and q_m were obtained from the plot connects ln q_e against ε^2 (Fig.7f) The E_{DR} values at different temperatures was found in between 1.1504-1.4012 kJ/mol, which are < 8 kJ/mol, indicating that the process follows physical adsorption [38].For the equilibrium study, the maximum sorption capacity was to be 1.262 mg/g by shrimp shell chitosan and 6.244 mg/g by crab shell chitosan for the Langmuir model which were reported by *Liao at al* [39] and *Halim et al*. [40] respectively,

for As(v) adsorption. *Guo et al.* [41] and *Poinern et al.*[42] reported the maximum sorption capacity of 31mg/g and 44.1mg/g by synthetic siderite and CNT-Ferrihydrite composite minerals respectively, for Langmuir model. Based on the above analysis, it was concluded that the Langmuir isotherm correlated better than Freundlich isotherms, suggesting monolayer adsorption. In our study, six different kinds of isotherms were applied to describe the equilibrium values. The maximum sorption capacity obtained from the Langmuir isotherm was 28.99mg/g. This result is comparable with the adsorption capacity of the other similar biosorbents reported in the literature [43].

Residual Mean Square Error (RMSE) analysis

The R^2 linear regression does not represent the errors in the isotherm curves. To evaluate the fit of the isotherm equations the RMSE analysis is employed.

$$\mathrm{RMSE} = \sqrt{\frac{1}{n-2}\sum_{i=1}^{n}(qe_{exp-}qe_{cal})^2} \quad (7)$$

$qe_{\exp}$, qe_{cal} and n are the experimental, calculated values and number of observations respectively. The smaller the RMSE value the better the curve fitting [44]. From Table 3, it assures that the process best fit was affirmed for Langmuir model.

Chi-square (χ^2) statistical test

The χ^2 test confirms the suitability of a particular isotherm model in describing the experimental data. The equation [45] is given as

$$\chi^2 = \sum \frac{(\mathrm{qe,exp} - \mathrm{qe,cal})^2}{\mathrm{qe,cal}} \quad (8)$$

The χ^2 value would be less if the adsorption data correlated concurs with experimental values. By which, from Table 3, the adsorption suitability more correlate with the Langmuir model than other models.

Adsorption kinetics modeling

The kinetics of As(v) adsorption onto the adsorbent were evaluated using the First order and pseudo-second order equations. The pseudo-first-order Lagergren equation in linear form [46] is expressed as Eq (9).

$$\log(\mathrm{qe} - \mathrm{qt}) = \log \mathrm{qe} - \frac{\mathrm{kt}}{2.303} \quad (9)$$

However, a pseudo-second-order equation analyzed the effective adsorption capacity, initial adsorption rate and the rate constant without any parameter in advance. The linear form of pseudo-second-order Lagergren equation [47] is shown as Eq (10).

$$\frac{\mathrm{t}}{\mathrm{qt}} = \frac{1}{\mathrm{k_2 qe^2}} + \frac{\mathrm{t}}{\mathrm{qe}} \quad (10)$$

The initial adsorption rate, h (mg/(g min)), as $t \to 0$, can be defined as:

$$\mathrm{h} = \mathrm{k_{2qe^2}} \quad (11)$$

The kinetic parameters were obtained through the Pseudo first order plot (Fig.S2), and second order plot (Fig.8). The higher regression coefficient value, 0.996, (Table 3) obtained from the second order model exposed its applicability in fitting the experimental kinetic data. From the Table 4, it shows that the h value of As(V) adsorption at 35ºC was higher than at 25ºC.

Intraparticle diffusion

The Weber-Morris model [48] for intraparticle diffusion explored the nature of the 'rate-controlling' step, which is given by the equation as

$$\mathrm{q_{id}} = \mathrm{k_{id}} t^{0.5} + \mathrm{c} \quad (12)$$

Where k_{id} is the intraparticle diffusion rate constant ($(mg/g\,min^{0.5})$). From the plots q_e versus $t^{0.5}$, Fig.S3, the relationship is not linear and follows rate-limiting step. The first sharper portion being rapid external surface adsorption, the second portion being gradual adsorption and the final phase being final equilibrium stage due to the low concentration of As(V) in the solution phase as well as less number of available adsorption sites.

Adsorption thermodynamics

The thermodynamic parameters ΔG, ΔH, and ΔS were utilized to elucidate the feasibility of adsorption. The Van't Hoff plot, Fig. 9 ($\ln K_c$ against 1/T) relates the parameters as

$$\ln \mathrm{K_c} = \frac{-\Delta \mathrm{H}}{\mathrm{RT}} + \frac{\Delta \mathrm{S}}{\mathrm{R}} \quad (13)$$

$$\Delta \mathrm{G} = -\mathrm{RT}\ln \mathrm{K_c} \quad (14)$$

Table 4: Kinetic parameters for As(v) adsorption onto CMC-EPI/INC composite at different temperatures.

Temp (K)	$q_{e,exp}$ mg/g	Pseudo first order			Pseudo Second order				Intra particle diffusion
		$q_{e,cal(mg/g)}$	$k_{1(min^{-1})}$	R^2	$h_{(mg/(g\,min))}$	$q_{e,cal}$ (mg/g)	$k_{1(min^{-1})}$	R^2	$k_{id\ (mg/g.min^{1/2})}$
298	1.1954	1.1698	0.0193	0.9805	0.1957	1.0169	0.2326	0.993	0.0448
303	1.2015	1.1985	0.0218	0.9873	0.2142	1.1278	0.2432	0.994	0.0422
308	1.2235	1.0356	0.0246	0.9925	0.2583	1.1705	0.1885	0.996	0.040

Table 5: Thermodynamic parameters for As(v) adsorption.

Van't Hoff plot			
Temp	ΔG $(kJ/_{mol})$	ΔH $(kJ/_{mol})$	ΔS $(kJ/_{mol/k})$
289K	-8.0787	7.9835	0.0539
303K	-8.3482		
308K	-8.6177		

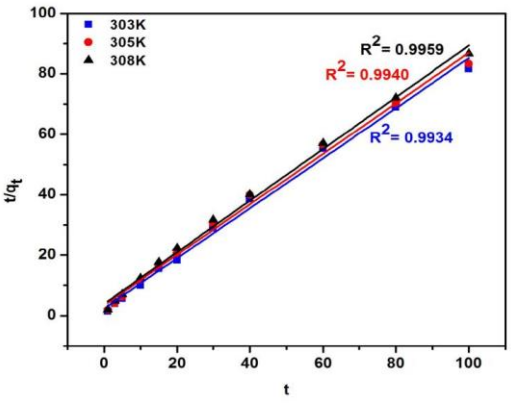

Fig.8 : Pseudo-second-order plot for As(V) adsorption.

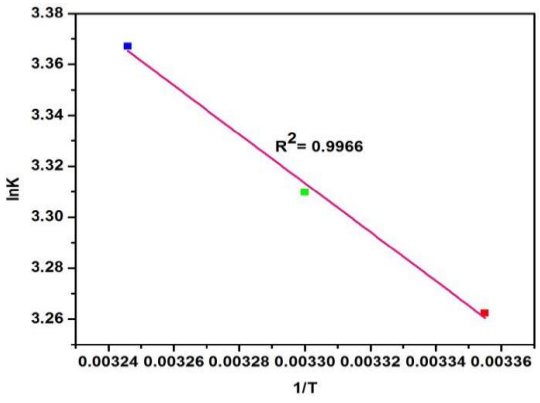

Fig. 9: Van't Hoffs plot for for As(V) adsorption.

Where K_c is the equilibrium constant, T the absolute temperature (K), and R is the universal gas constant (8.314J/mol k). The calculated values of the energy parameters ΔG, ΔH, and ΔS are given in the Table 5. The negative ΔG values observed at various temperatures suggested the feasibility and spontaneous adsorption process. The positive nature and the value of ΔH= 7.9835 KJ/mol/k, which was < 80 KJ/mol/k suggesting that the reaction follows endothermic physisorption. The positive value of ΔS reflects the affinity and some structural changes in adsorbent and adsorbate during adsorption process.

Effect of competing anions

The adverse effect of challenging anions in the arsenic adsorption was investigated with 0.5,1,5,10 and 20 mg/L of N(asNo_3^-), P (as PO_4^{3-}) and Si(asSiO_3^{2-}) with an initial As(V) concentration of 2.0mg/L at 35'c. The results are shown in Table S1. The anions hostile effect on As(V) removal decreased in the following order, $SiO_3^{2-} > PO_4^{3-} > No_3^-$.

None of the anions had serious adverse effect except Si as SiO_3^{2-}. The N as No_3^- and P as PO_4^{3-} has little adverse effects on amounts to a 3.70% and 5.29% whereas Si as SiO_3^{2-} radically decreased up to 8.99% adsorption respectively at 20mg/L. The observed reduction percentage due to Si as SiO_3^{2-} was less compared with other reports of *Zhang et al*. [49], and *Guo et al.* [50], encountered 30% and 26% reduction respectively. This could be due to the strong complexation of arsenate with oxidized iron and chitosan which are the major significance of the prepared adsorbent.

Desorption experiments

Desorption studies carried out with 0.1M NaOH, after adsorption of As(V) having initial concentration of 10 ppm in a batch reactor. The adsorption-desorption cycle was repeated four times using the same affinity adsorbent to find the reusability of the adsorbent. The desorption result (Table S2), revealed that after four cycles around 81-87% of loaded As(v) were found to be desorbed during desorption cycles. The desorption ratio was calculated by:

$$R(\%) = \frac{C_2}{C_0 - C_1} \times 100\% \quad (15)$$

Where C_0, C_1, and C_2 are the initial, equilibrium concentration of adsorbed and desorbed solution in mg/L respectively.

Applicability to arsenic-contaminated waste water

As(v) contaminated pesticide wastewater having an initial concentration of 124µg/L was subjected to adsorption at the optimal conditions. The results found that As(v)ion was not detected after treatment. It is evident that the removal of arsenic down to WHO drinking standards were achieved by synthesized adsorbent.

CONCLUSIONS

In this study, a novel iron doped chitosan biosorbent was prepared, characterized and evaluated for arsenic removal. The equilibrium data could be described by the Langmuir and Dubini-Raduskhevich (D-R) isotherms. The maximum sorption capacity for As(v) was calculated to be 28.99 mg/g from the Langmuir isotherm and follows pseudo-second-order kinetics. Thermodynamic studies revealed the process is spontaneous, endothermic and physisorption in nature. Interfering ions had marginal effects on adsorption. The adsorbent was successfully recycled for four cycles and efficiently treated As(v) contaminated wastewater. Thus, it could be concluded that the CMC-EPI/INC biosorbent would be a potential candidate for arsenic filtering units, due to its biocompatibility.

Acknowledgements

The authors also would like to thank Department of Chemistry, IIT Madras and Center for Environment, CLRI Chennai for providing the analytical instrumentation facility. One of the authors Dr. G. Prabha would like to thank University Grant Commission (UGC), Government of India, for providing the fund under the scheme of UGC – Dr. D.S. Kothari Postdoctoral Fellowship (Award No:F.4-2/2006(BSR)/CH/18-19/0110).

Received : Mar. 28, 2022 ; Accepted : Jun. 13, 2022

REFERENCES

[1] Hering J.G., Katsoyiannis I.A., Theoduloz G.A., Berg M., Hug S.J., Arsenic Removal from Drinking Water: Experiences with Technologies and Constraints in Practice, *Journal of Environmental Engineering*, **143**: 1-9 (2017).

[2] Sharma A.K., Tjell J.C., Sloth J.J., Holm P.E., Review of Arsenic Contamination, Exposure through Water and Food and Low Cost Mitigation Options for Rural Areas, *Applied Geochemistry*, **41**: 11–33 (2014).

[3] Jain CK, Ali I. Arsenic: Occurrence, Toxicity and Speciation Techniques, *Water Research*, **34(17)**: 4304-4312 (2000)

[4] Morton W. E., Dunette D. A., "Arsenic in the Environment, Part II: Human and Health and Ecosystem Effects", Wiley and Sons Inc., New York: 17-34 (1994).

[5] "Drinking water Quality Information, World Health Organization", Vol 2, Second Edition, WHO, Geneva: 940-949 (1984).

[6] Katsoyiannis I.A., Voegelin A., Zouboulis A.I., Hug S.J., Enhanced As(III) Oxidation and Removal by Combined Use of Zero Valent Iron and Hydrogen Peroxide in Aerated Waters at Neutral pH Values, *Journal of Hazardous Material*, **297**: 1–7 (2015).

[7] Wei Y., Yu X., Liu C., Ma J., Wei S., Chen T., Yin K., Liu H., Luo S. Enhanced Arsenite Removal from Water by Radially Porous Fe-Chitosan Beads: Adsorption and H_2O_2 Catalytic Oxidation, *Journal of Hazardous Material*, **373**: 97–105 (2019).

[8] Yang J., Hou B., Wang J., Tian B., Bi J., Wang N., Li X., Huang X., Nanomaterials for the Removal of Heavy Metals from Wastewater, *Nanomaterials*, **9(3)**: 424-462 (2019).

[9] Genc-Fuhrman H., Tjell J. C., McConhie D., Increasing the Arsenate Adsorption Capacity of Neutralized Red Mud (Bauxsol), *Journal of Colloid Interface Science*, **27(2)**: 313-320 (2004).

[10] Gupta K., Joshi P., Gusain R., Khatri O P., Recent Advances in Adsorptive Removal of Heavy Metal and Metalloid Ions by Metal Oxide-Based Nanomaterials, *Coordination Chemistry Reviews*, **445**: 214100 (2021).

[11] Azimi A., Azari A., Rezakazemi M., Ansarpour M., Removal of Heavy Metals from Industrial Wastewaters: A Review, *Chem. Bio. Eng. Rev.*, **4**: 37–59 (2017).

[12] Juang R.S., Wu F.C., Tseng R.L., Adsorption Removal of Copper (II) Using Chitosan from Simulated Rinse Solutions Containing Chelating Agents, *Water Research*, **33(10)**: 2403-2409 (1999).

[13] Anjum M., Miandad R., Waqas M., Gehany F., Barakat M., Remediation of Wastewater Using Various Nano-Materials, *Arabian Journal of Chemistry*, **12**: 4897–4919 (2019).

[14] Gimenez J., Martinez M., de Pablo., Arsenic Sorption onto Natural Hematite, Magnetite, and Goethite, *Journal of Hazardous Material*, **141**: 575-580 (2007).

[15] Bilal M., Jing Z., Zhao Y., Iqbal HM., Immobilization of fungal Laccase on Glutarldehyde Cross-Linked Chitosan Beads and its Bio-Catalytic Potential to Degrade Bisphenol A, *Biocatalysis and Agricultural Biotechnology*, **19**: 101174-101184 (2019).

[16] Gutha Y., Zhang Y., Zhang W., Jiao X., Magnetic - Epichlorohydrin Crosslinked Chitosan Schiff's Base (m-ECCSB) as a Novel Adsorbent for the Removal Of Cu(II) Ions from Aqueous Environment, *International Journal of Biological Macromolecule*, **97**: 85-98 (2017).

[17] Marrakchi F., Khanday W.A., Asif M., Hameed B.H., Cross-Linked Chitosan/Sepiolite Composite for the Adsorption of Methylene Blue and Reactive Orange 16, *International Journal of Biological Macromolecule*, **93(pt A)**: 1231-1239 (2016).

[18] Zhu L.Y., Zhu Z.L., Qiu Y.L., Zhang R.H., Synthesis of As (V)-Cr (III) Co-Imprinted Polymer and its Adsorption Performance for Arsenate Species, *Separation Science Technology*, **49**: 1584–1591 (2014).

[19] Fierro V., Muniz G., Ballinas M.L., Arsenic Removal by Iron-Doped Activated Carbons Prepared by Ferric Chloride Forced Hydrolysis, *Journal of Hazardous Material*, **168(1)**: 430-437 (2009).

[20] Genc-Fuhrman H., Tjell J.C., McConchie D., Adsorption of Arsenic from Water Using Activated Neutralized Red Mud, *Environment Science and Technology*, **38(8)**: 2428-2429 (2004).

[21] Appelo C.A.J., Van der Weiden M.J.J., Tournassat C., Charlet L., Surface Complexation of Ferrous Iron and Carbonate on Ferrihydrite and the Mobilization of Arsenic, *Environment Science and Technology*, **36(14)**: 3096-3107 (2002).

[22] Vieira R.S., Beppu M.M., Interaction of Natural and Crosslinked Chitosan Membranes with Hg (II) Ions, *Colloids and Surfaces A*, **279(1-3)**: 196-207 (2006).

[23] Guibal E., Vincent T., Navarro R., Metal Ion Biosorption on Chitosan for the Synthesis of Advanced Materials, *Journal of Material Science*, **49**: 5505-5518 (2014).

[24] Song X., Li L., Geng Z., Zhou L., Ji L., Effective and Selective Adsorption of As(III) Via Imprinted Magnetic Fe_3O_4/HTCC Composite Nanoparticles, *Journal of Environment Chemical Engineering*, **5**: 16–25 (2017).

[25] Viswanathan N., Meenakshi S., Enhanced Fluoride Sorption Using La(III) Incorporated Carboxylated Chitosan Beads, *Journal of Colloid Interface Science*, **322**: 375–383(2008).

[26] Viswanathan N., Meenakshi S., Selective Sorption of Fluoride Using Fe(III) Loaded Carboxylated Chitosan Beads, *Journal of Fluorine Chemistry*, **129**: 503–509 (2008).

[27] Viswanathan N., Meenakshi S., Zr(IV) Loaded Cross-Linked Chitosan Beads With Enhanced Surface Area for the Removal of Nitrate and Phosphate, *Colloids Surfaces B*, **72** : 88–93 (2009).

[28] Viswanathan N., Sundaram C.S., Meenakshi S., Removal of Fluoride from Aqueous Solution Using Protonated Chitosan Beads, *Journal of Hazardous Material*, **161**: 423–430 (2009).

[29] Ngah W.S.W., Ghani S.A, Kamari A., Adsorption Behaviour of Fe(II) and Fe(III) Ions in Aqueous Solution on Chitosan and Cross-Linked Chitosan Beads, *Bioresource Technology*, **96**: 443–450 (2005).

[30] Hosseini S.M., Younesi H., Bahramifar N., Mehraban Z., A Novel Facile Synthesis of the Amine-Functionalized Magnetic Core Coated Carboxylated Nanochitosan Shells as an Amphoteric Nanobiosupport, *Carbohydrate Polymers*, **221**: 174-185 (2019).

[31] Manzoor K., Ahmad M., Ahad S., Ikram S., Removal of Pb(II) and Cd(II) from Waste Water Using Arginine Cross-Linked Chitosan-Carboxymethyl Cellulose Beads as a Green Adsorbent, *RSC Advances*, **9**: 7890-7902 (2019).

[32] Monier M., Abdel-Latif D.A., Fabrication of Au (III) Ion-Imprinted Polymer Based on Thio-Modified Chitosan, *International Journal Biological Macromolecule*, **105(1)**: 777-787 (2017).

[33] Kumar A.S.K., Kalidhasan S., Rajesh V., Rajesh N., Application of Cellulose-Clay Composite Biosorbent Toward the Effective Adsorption and Removal of Chromium from Industrial Waste Water, *Industrial Engineering Chemical Research*, **51**: 58-69 (2012).

[34] Zhou S., Xue Y., Zhao Y., Wang Q.,Chen Y., Li M., Xing W., Competetive Adsorption of Hg^{2+},Pb^{2+} and Co^{2+} Ions on Polyacrylamide/Attapulgite, *Desalination*, **270**: 269-274 (2011).

[35] Wang J.L., Chen C., Biosorbents for Heavy Metals Removal and their Future, *Biotechnology Advances*, **27**: 195-226 (2009).

[36] Connell W.O., Birkinshaw C.,O'Dwyer T.F., Heavy Metal Adsorbents Prepared from the Modification of Cellulose: A Review, *Bioresource Technology*, **99(15)**: 6709-6724 (2008).

[37] Ayawei N., Ekubo A.T., Wankasi D., Dikio E.D. Adsorption of Congo Red by Ni/Al-CO_3: Equilibrium, Thermodynamic and Kinetic Studies, *Oriental Journal of Chemistry*, **5(03)**: 56-70 (2015).

[38] Sharma S., Bharathi M., Rajesh N., Efficacy of a Heterocyclic Ligand Anchored Biopolymer Adsorbent for the Sequestration of Palladium, *Chemical Engineering Journal*, **59**: 457-466 (2015).

[39] Chia-Pin C., Ming-Chao L., Chung-Min L., Low-Cost Farmed Shrimp Shells Could Remove Arsenic From Solutions Kinetically, *Journal of Hazardous Material*, **171(1-3)**: 859-864 (2009).

[40] Rana M.S., Halim M.A., Waliul H., Kamrul H., Hossain M.K., Bioadsorbtion of Arsenic by Prepared and Commercial Crab Shell Chitosan, *Biotechnology*, **8(1)**: 160-166 (2009).

[41] Guo H., Li Y., Zhao K., Arsenate Removal from Aqueous Solution Using Synthetic Siderite, *Journal of Hazardous Material*, **176(1-3)**: 174-180 (2010).

[42] Yuwei C., Jianlong W., Preparation and Characterization of Magnetic Chitosan Nanoparticles and its Application for Cu (II) Removal, *Chemical Engineering Journal*, **168(1)**: 286-292 (2011).

[43] Poinern G.E.J., Parsonage D., Touma B., Issa Ghosh M.K., Paling E., Singh P., Preparation, Characterization and As(V) Adsorption behavior of CNT-Ferrihydrite Composites, *International Journal of Engineering Science and Technology*, **2(8)**: 13-24 (2010).

[44] Krishna Kumar A.S., Uday Kumar C., Vidhya R., Rajesh N., Microwave Assisted Preparation of N-Butyl Acrylate Grafted Chitosan and its Application for Cr (VI) Adsorption, *International Journal of Biological macromolecule*, **66**: 135-143 (2014).

[45] Anjali G., Yunus M., Nalini S., Zerovalent Iron Encapsulated Chitosan Nanospheres: A Novel Adsorbent for the Removal of Total Inorganic Arsenic from Aqueous Systems, *Chemosphere*, **86(2)**: 150-155 (2012).

[46] Choudhary B., Paul D., Isotherms, Kinetics and Thermodynamics of Hexavalent Chromium Removal Using Biochar, *Journal of Environment Chemical Engineering*, **6(2)**: 2335–2343 (2018).

[47] Foo K.Y., Hameed B.H., Insights into the Modeling of Adsorption Isotherm Systems, *Chemical Engineering Journal*, **156(1)**: 2–10 (2010).

[48] Weber Jr, W.J., Morris J.C., Kinetics of Adsorption on Carbon from Solution, *Journal of the Sanitary Engineering Division*, **89**: 31-42 (1963).

[49] Zhang W., Singh P., Paling E., Delides S., Arsenic Removal from Contaminated Water by Natural Iron Ores, *Mineral Engineering*, **17**: 517-524 (2004).

[50] Guo H.M., Stuben D., Berner Z., Removal of Arsenic from Aqueous Solution by Natural Siderite and Hematite, *Applied Geochemistry*, **22(5)**: 1039-1051 (2007).